Hindawi
Geofluids
Volume 2022, Article ID 9390589, 16 pages
https://doi.org/10.1155/2022/9390589

Research Article

Quantification of Pore Size and Movable Fluid Distribution in Zhangjiatan Shale of the Ordos Basin, China

Jing Xu,[1,2] Yunjin Ge,[2] Yonghong He,[2] Renhai Pu,[1] Linyu Liu,[1] Kefeng Du,[2] Hongjin Li,[2] Xiao He,[2] and Liang Duan[1]

[1]*State Key Laboratory of Continental Dynamics and Department of Geology, Northwest University, Xi'an, 710069 Shaanxi, China*
[2]*Research Institute of Shaanxi Yanchang Petroleum Group Co., Ltd., Xi'an, 710075 Shaanxi, China*

Correspondence should be addressed to Yunjin Ge; 121853731@qq.com and Liang Duan; duanl@nwu.edu.cn

Received 7 May 2022; Revised 27 June 2022; Accepted 1 July 2022; Published 15 July 2022

Academic Editor: Wenhui Li

The Triassic Zhangjiatan shale in the Ordos basin, recognized as one of most promising shale oil and gas resources in China, is one example of medium-low-maturity lacustrine shale reservoirs wherein the pore network has been proven to be different from those of both conventional and high-maturity marine shale reservoirs. Here, we examine the quantitative characterization of pore size and movable fluid distribution of the Zhangjiatan shale reservoir. Eight shale core plugs were measured in a series of nuclear magnetic resonance (NMR) experiments to determine the pore structure and pore fluid transport during the processes of centrifuging and heating. The complete pore size distribution was obtained from the T_2 spectrum by integrating NMR, high-pressure mercury intrusion, and nitrogen gas adsorption. The results show that the movable fluid saturation of Zhangjiatan shale is 19.47–33.02% and the capillary-bound fluid saturation is 14.53–27.62%, whereas the unrecoverable fluid saturation was 43.51–65.26%. The movable fluids are mainly detected in macropores and mesopores with a minimum pore size of 50.5–121.2 nm, while capillary-bound fluids are mainly found in small pores and some mesopores with a minimum size of 25.8–67.5 nm. Almost all unrecoverable fluids are in micropores and small pores. In contrast to high-maturity shale reservoirs, the Zhangjiatan shale shows a poor correlation between total organic carbon content and unrecoverable fluid saturation but a good correlation between clay minerals and unrecoverable fluid saturation, showing that most micropores are associated with clay minerals and the organic matter pores are less developed. This study provides an accurate determination of the pore size distribution and pore fluid typing of Zhangjiatan shale, which is of great significance for the development of high-quality but medium-low-maturity shale reservoirs in China.

1. Introduction

Shale reservoirs have long been known and exploited as source rocks, but they still contain a large amount of oil and gas reserve that can now be produced by using modern but unconventional techniques such as horizontal drilling and hydraulic fracturing. With the breakthrough of shale exploration in North America (e.g., Barnett, Marcellus, and Horn River), shale reservoirs have become the giant resources for the 21st Century [1] and the major contributor to the global growth of natural gas and crude oil production [2, 3]. It is shown that the effective porosity, pore fluid movability, pore size distribution, and petroleum geochemistry of shale reservoirs are an important basis for evaluating their reservoir capacity for shale oil and gas [4–6], and most studies on shale reservoir capacity in recent years have been focused on high maturity marine shale reservoirs or lacustrine shale reservoirs with the vitrinite reflectance (R_o) greater than 1.0% [7–9]. Compared to well-studied high-maturity marine shales, medium-low-maturity ($R_o = 0.5 - 1.0\%$) lacustrine shales are different in terms of its geological settings and reservoir characteristics and less explored and developed globally. Therefore, our understanding of their reservoir capacity, especially the accurate determination of pore size and movable fluid distribution, is still limited.

It has proven that medium-low-maturity shales have fewer organic pores and are characterized by the occurrence

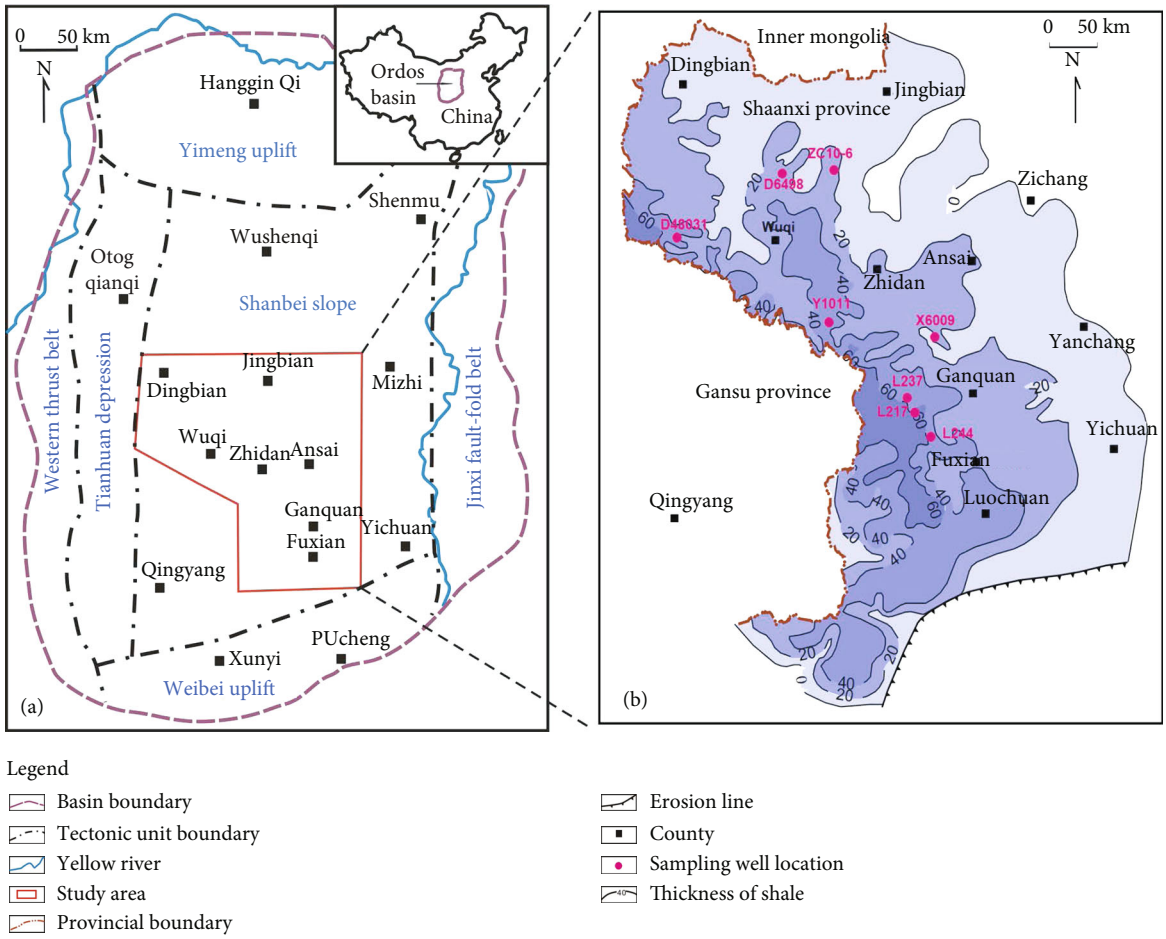

Figure 1: Map of the Ordos basin in central China (a) and isopach map of Zhangjiatan shale in the lower part of Member 7 of the Upper Triassic Yanchang Formation with coring well locations (b).

of interparticle pores, intraparticle pores, and a small number of organic matter pores and microfractures [10]. It is well known that the pore size distribution controls the transport behavior of fluids through pores [11]. The pore fluids are usually classified into two, namely, movable and bound fluids, and bound fluids are further classified as capillary-bound and clay-bound fluids [12, 13]. In a generally accepted definition of sandstones or carbonate rocks, the clay-bound porosity is not part of the effective porosity and is the difference between the total porosity and effective porosity [14]. However, the studies of shales have indicated that many nanopores in shales are paragenetic not only with the clay minerals but also with organic matter [10]. Considering that we cannot determine whether the so-called "clay-bound fluid" occurs in the clay minerals of shales or not, in this study, we defined the difference between the total porosity and effective porosity as the unrecoverable porosity. Therefore, the pores with movable and capillary-bound fluids are identified as effective pores, whereas clay-bound fluids are defined as unrecoverable fluid. Moreover, fluid movability is not only related to the pore structure, but the proportion of movable fluid becomes higher as the temperature increases [15]. Therefore, using only nuclear magnetic resonance (NMR) and centrifugation to evaluate pore fluid movability may underestimate the effective porosity and ultimate recovery of shale reservoirs [16]. A recent study by Testamanti and Rezaee [16] improved the traditional centrifugation method by heating shale samples to further extract the capillary-bound fluids from the pores such that these fluids are rapidly discharged. Nevertheless, with a further increase in the temperature, it becomes increasingly difficult to remove the fluids from the tiny pores of the shales, and the remaining fluids can be inferred as unrecoverable.

The Zhangjiatan shale, which is the shale in the lower part of Member 7 of the Upper Triassic Yanchang Formation in the southeastern Ordos basin (Figure 1), is representative of the medium-low-maturity shale reservoir that has been recognized as one of the most promising shale oil and gas resources in China [17]. Here, we report the results of a series of NMR experiments conducted on core plugs of Zhangjiatan shale with different maturity levels to determine the pore structure and pore fluid transport during the processes of centrifuging and heating. The quantitative determination of pore size and movable fluid distribution of the Zhangjiatan shale provides the basis for an in-depth discussion on its reservoir capacity and development of high-quality but medium-low-maturity shale reservoirs.

Table 1: TOC, R_o, and mineral compositions of eight shale core plugs.

Sample	Depth (m)	TOC (%)	R_o (%)	Main mineral composition (%)								
				Quartz	Clay minerals	Plagioclase	Potassium feldspar	Mica	Calcite	(Iron) dolomite	Pyrite	Siderite
L237	1176.9	3.96	0.55	24.4	32.7	7.9	14.8	1.3	8.6	5	3.8	1.5
L244	1314	3.72	0.58	40.7	24.6	7.2	18.7	1.4	2.4	2.1	2.9	0
L217	1379.7	5.33	0.74	39	26.2	5.6	24.2	0.9	0	1.6	1.1	1.4
X6009	1410	3.48	0.82	21.8	18.2	14.4	40.5	0.6	1.8	1.7	0	1
Y1011	1747	5.78	0.56	24.2	36.1	9.7	11.5	0	3.1	2.5	9.7	3.2
ZC10-6	2078	5.15	0.89	34.7	35	4.2	15.3	2.1	2.4	2.1	2.5	1.7
D6498	2230.5	1.75	0.99	51.4	18.9	4.1	22.7	1.7	1.2	0	0	0
D48031	2496	6.54	1.05	24.7	31	3.6	10.1	0	1.6	1.5	25.8	1.7

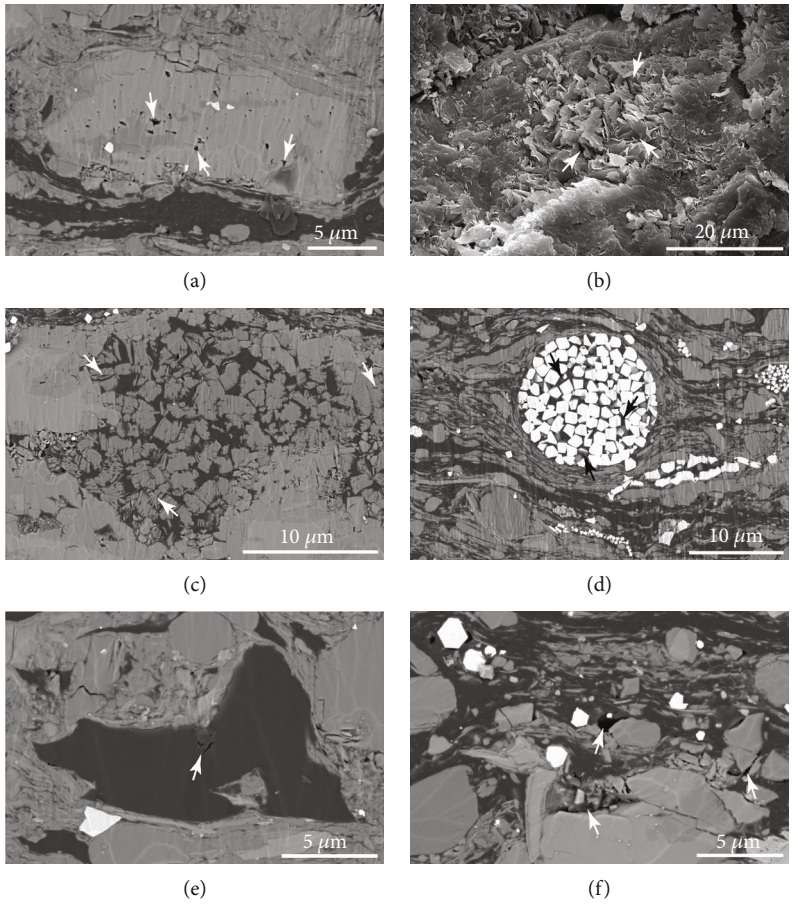

Figure 2: Secondary electron images of milled surfaces showing various pores in Zhangjiatan shale. (a) Intraparticle dissolution pores (white arrows) in feldspar. Sample L217. (b) Interparticle pores (white arrows) in illite-smectite mixed-laminae. Sample X6009. (c) Interparticle pores (white arrows) in kaolinite laminae. Sample D48031. (d) Intercrystalline pores (black arrows) in pyrite framboids. Sample D48031. (e) Organogenic pores (white arrow). Sample L217. (e) Preserved interparticle pores (white arrows) and microfractures. Sample D48031.

2. Geological Setting

The Ordos basin is the second largest petroliferous sedimentary basin in China, and it is located in the western part of the North China craton. The basin became an interior lake basin during the Mesozoic, and up to 4000 m of terrestrial facies siliciclastic rocks were accumulated from Triassic to Cretaceous. The study area is located on the central and southern part of the Shanbei slope of the Ordos basin (Figure 1), which is a west-dipping monocline with a 0.5-degree dip angle in which seismically identifiable faults and local low-relief folds are absent [18].

The Upper Triassic Yanchang Formation contains fluviolacustrine siliciclastic rocks ranging from 900 to 1600 m

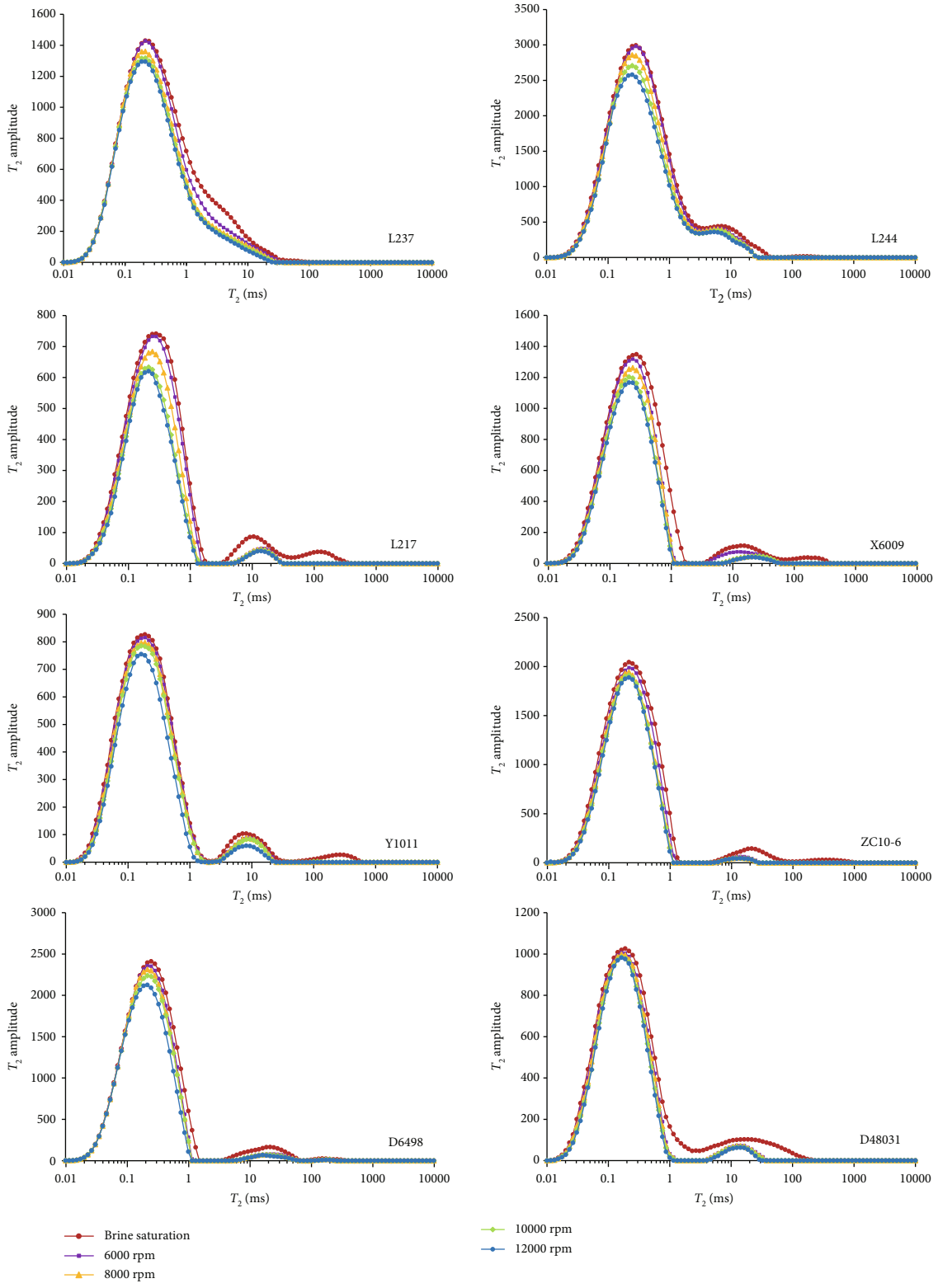

Figure 3: NMR T_2 spectrum distributions of shale samples under 100% brine-saturated and centrifugal conditions.

in thickness, and it can be subdivided into 10 members. The Zhangjiatan shale is in the lower part of Member 7, and it is currently considered to be one of the most prolific hydrocarbon source rocks in the Ordos basin and the most promising target for shale oil and gas exploration in China. The shale was formed at the most expansive stage of the lacustrine basin and developed in a semideep to deep lacustrine environment [19, 20]. It is up to 60 m thick in the study area (Figure 1) and contains types I and II_1 organic matter [19, 21]. Organic matter in the Zhangjiatan shale has a low

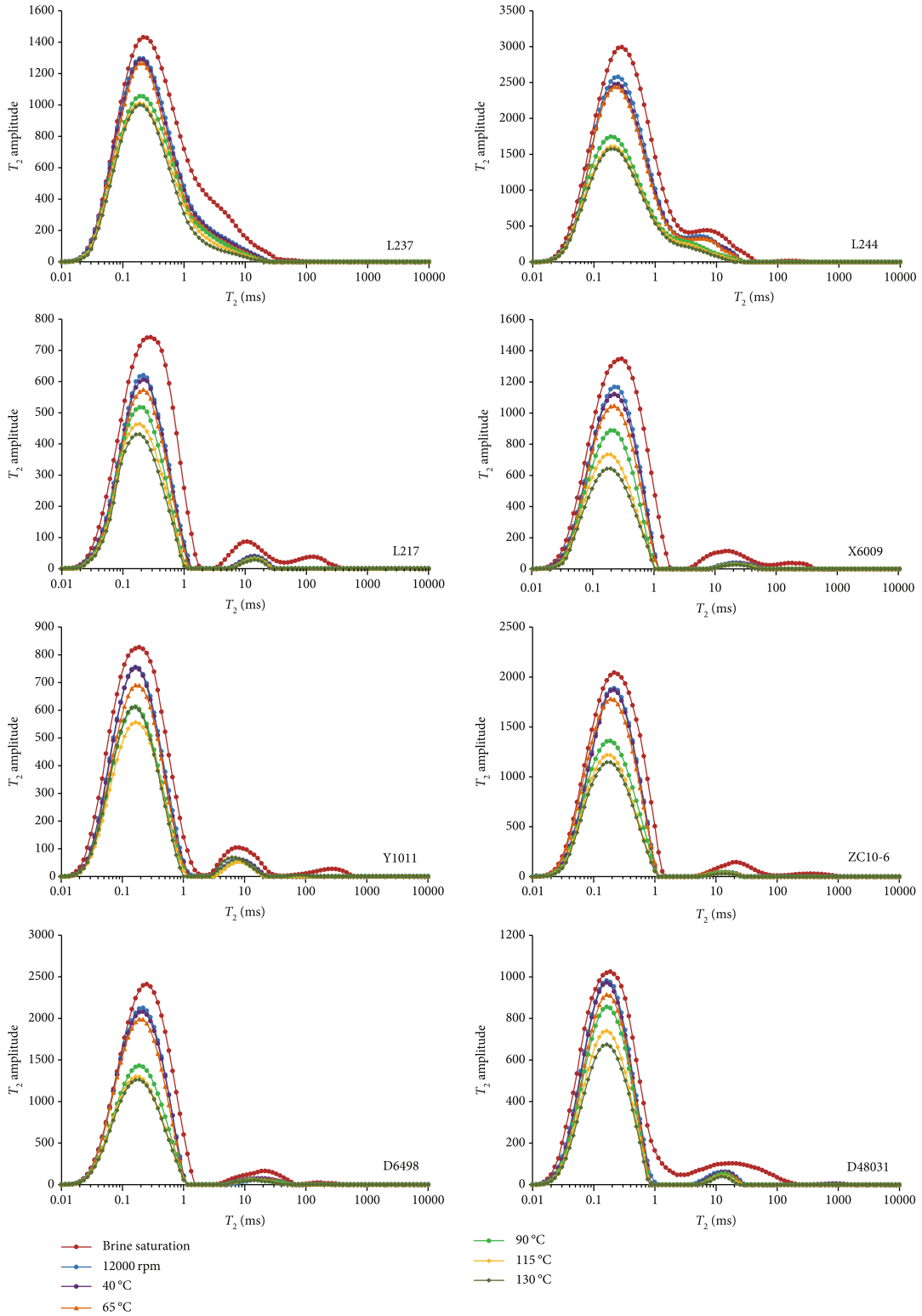

Figure 4: NMR T_2 spectrum distributions of shale samples under brine-saturated and heat-treated.

thermal maturity as indicted by R_o values that are commonly less than 1.3% [22, 23]. There is a long history of hydrocarbon production from the Zhangjiatan shale, and both the rate of oil and gas production and estimate of ultimate recoverable reserves have increased in recent years.

3. Dataset and Methodology

As an important oil and gas producing area in the Ordos basin, tens of thousands of boreholes penetrate the Upper Triassic Zhangjiatan shale in the Shanbei slope. In this

Table 2: T_2 cutoff values, pore fluid saturation, porosity, and permeability observed from Zhangjiatan shale samples.

Sample	R_o (%)	T_{2-1} (ms)	T_{2-2} (ms)	S_m (%)	S_c (%)	S_u (%)	φ (%)	φ_m (%)	φ_c (%)	φ_u (%)	K (mD)	Pore volume (ml/g)
L237	0.55	1.1	0.5	20.21	14.53	65.26	2.68	0.54	0.39	1.75	0.0003	0.04721
L244	0.58	1.01	0.36	19.47	25.11	55.42	6.08	1.18	1.53	3.37	0.0054	0.05137
L217	0.74	0.4	0.25	33.02	17.99	49	4.81	1.59	0.87	2.36	0.0116	0.09771
X6009	0.82	0.43	0.21	28.87	27.62	43.51	3.13	0.9	0.87	1.36	0.0016	0.06219
Y1011	0.56	0.41	0.23	22.8	16.38	60.82	2.91	0.66	0.48	1.77	0.0006	0.04861
ZC10-6	0.89	0.44	0.25	22.24	20.15	57.61	3.76	0.84	0.76	2.17	0.0019	0.05629
D6498	0.99	0.49	0.25	20.07	25.07	54.86	2.47	0.5	0.62	1.35	0.0002	0.04214
D48031	1.05	0.42	0.21	24.61	20.7	54.69	2.53	0.62	0.52	1.38	0.0004	0.03132

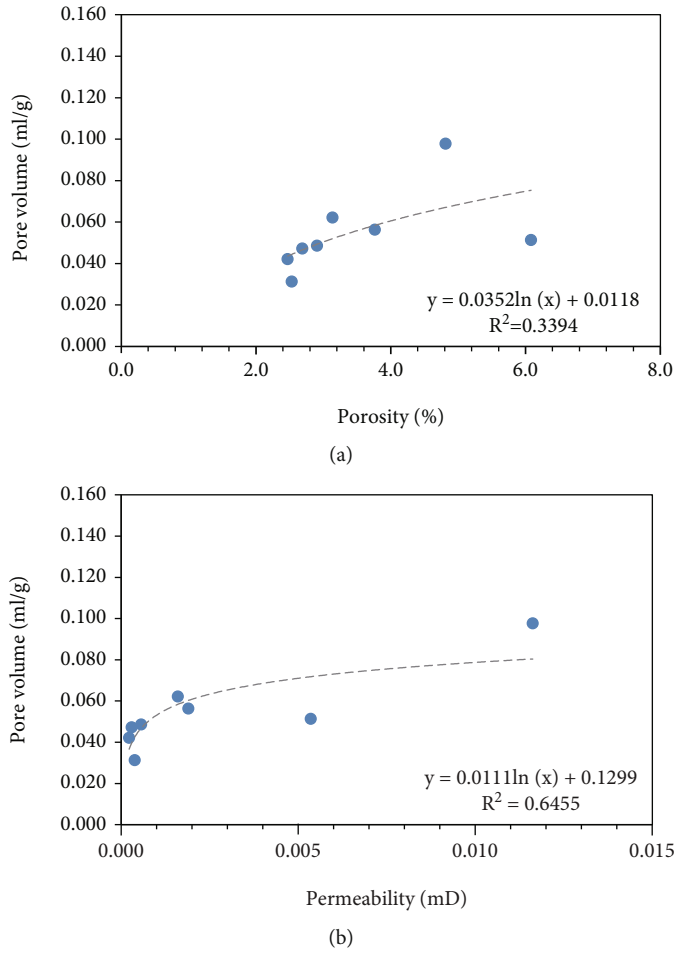

Figure 5: Overall positive correlations between measured shale pore volume and total porosity and permeability.

paper, we focus on shale core plugs collected from eight boreholes labelled as L237, L244, L217, X6009, Y1011, ZC10-6, D6498, and D48031. The organic carbon content (TOC), vitrinite reflectance (R_o), SEM, field-emission SEM (FE-SEM), and X-ray diffraction (XRD) analyses of whole-rock mineral composition of shale samples collected at different depths were conducted at first. Among the samples collected at different depths, eight shale samples with different organic matter maturity levels (Table 1) were selected for NMR, gas adsorption, and high-pressure mercury intrusion experiments, to quantitatively characterize the pore fluid movability and pore size distribution of the shale reservoir.

3.1. NMR Experiments. The low-field NMR is a commonly used method to accurately analyze pore characteristics and the fluid distribution of samples without destruction [24]. NMR time spectrum (T_2 spectrum) relaxation contains information on the structures and distributions of rock pores and the fluids inside these pores, which can be used to estimate pore fluid movability, pore size distribution, and permeability [25–27].

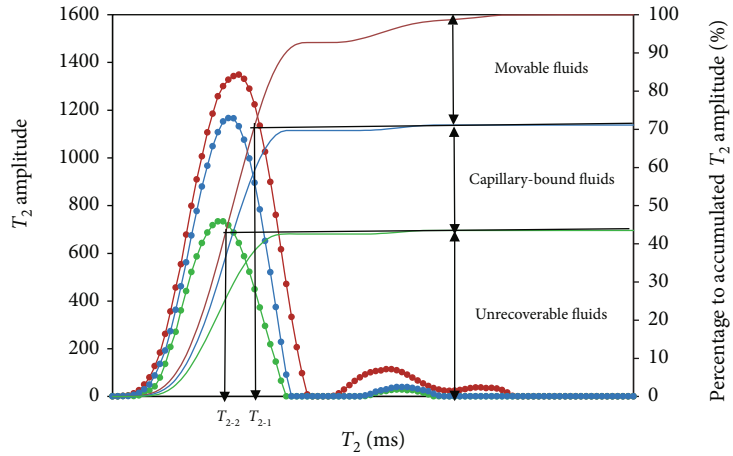

FIGURE 6: Method for calculating T_2 cutoff values and differentiating pore fluids using incremental and cumulative T_2 spectral curves. The red solid curves with dots and solid curves represent the incremental and cumulative T_2 spectrum under 100% brine-saturated condition. The blue solid curves with dots and solid curves represent the incremental and cumulative T_2 spectrum after centrifugation at 12000 rpm. The green solid curves with dots and solid curves represent the incremental and cumulative T_2 spectrum after heating to the threshold temperature.

The NMR experiments in this study were conducted using a MesoMR12-040 NMR spectrometer, and the amplitude curves of the transverse relaxation time T_2 were obtained from 0.01 ms to 10000 ms at 60 log intervals using a weak magnetic field (0.5 ± 0.08 T). The waiting time adopted was 1500 ms, and 128 scans were conducted.

Before the experiments, the eight samples were processed into standard cylindrical cores of 25 mm in diameter and 35–50 mm in length. A series of NMR experiments were conducted on these eight samples under full brine saturation, centrifugation, and heat treatment conditions to analyze the pore fluid transport during centrifugation and heat treatments. The detailed procedures are described as follows.

Firstly, wash the remaining oil and salt away from the rock sample, and dry and cool the sample to a constant temperature of 65°C. Measure the gas adsorption to understand the porosity of the sample. Then, the samples were saturated with pressurized brine (resembling formation water), and NMR measurements were collected for the saturated samples. Saturating the samples with brine minimized the water-sensitive effects of clay minerals on the experimental results. Thirdly, NMR experiments under centrifugation were performed, and the rock samples were centrifuged at high speeds for 3 h at 6000 rpm, 8000 rpm, 10000 rpm, and 12000 rpm (corresponding to centrifugal pressures of 1.42 MPa, 2.52 MPa, 3.94 MPa, and 5.68 MPa, respectively). Subsequently, NMR measurements were performed to obtain the T_2 spectra of the centrifuged rock samples at all speeds. Finally, all shale samples were subjected to heat treatments and NMR experiments. Each shale sample was subjected to cyclic heat treatments from low to high temperatures in a sequence of 40°C, 65°C, 90°C, 115°C, and 130°C. The heated sample was cooled to room temperature for NMR measurements to obtain a T_2 spectrum at each temperature point.

3.2. High-Pressure Mercury Intrusion Porosimetry (MIP). The MIP method is a common experimental method to analyze pore size distributions of shales. According to Washburn's equation [28], the corresponding pore radius r can be obtained for each intrusion pressure P, such that the amount of injected mercury for each pore radius can be determined to obtain the corresponding pore volume and pore size distribution [28] However, mercury does not easily enter the micropores and mesopores of shales, and the high pressure will cause the deformation of shale pores. These, in turn, affect the experimental results [29]. Therefore, the high-pressure mercury intrusion method is mainly used to analyze mesopores and macropores. In this paper, the experiments were conducted using a fully automatic mercury piezometer, AUTOPORE IV9500, manufactured by Conta, USA, with a maximum injection pressure of 200 MPa and a pore size measurement range of 0.007–360 μm.

3.3. N_2 Gas Adsorption. The N_2 adsorption method has been mainly used to examine the distribution characteristics of small pores and pores larger than 2 nm in shales. In this research, a fully automatic specific surface area and porosity analyzer, Micromeritics Instrument TriStar II 3020, was used for pore size distribution measurements. The pore sizes of the samples were in the range of 60–80 mesh. Before the experiments, the samples were degassed in a vacuum at 150°C for 3 h. After that, adsorption-desorption curves were obtained by using high-purity nitrogen as the adsorbent at a relative pressure of 0–0.995 and a liquid nitrogen temperature (77.3 K). Subsequently, the pore volumes and pore size distributions were obtained using the Barrett-Joyner-Halenda pore calculation model.

4. Results

4.1. Characteristics of Shale Samples. It is shown that the TOC contents of the shale samples range from 1.75% to 6.54%, and the R_o values lie between 0.55% and 1.05% (Table 1), suggesting that the Zhangjiatan shale are of

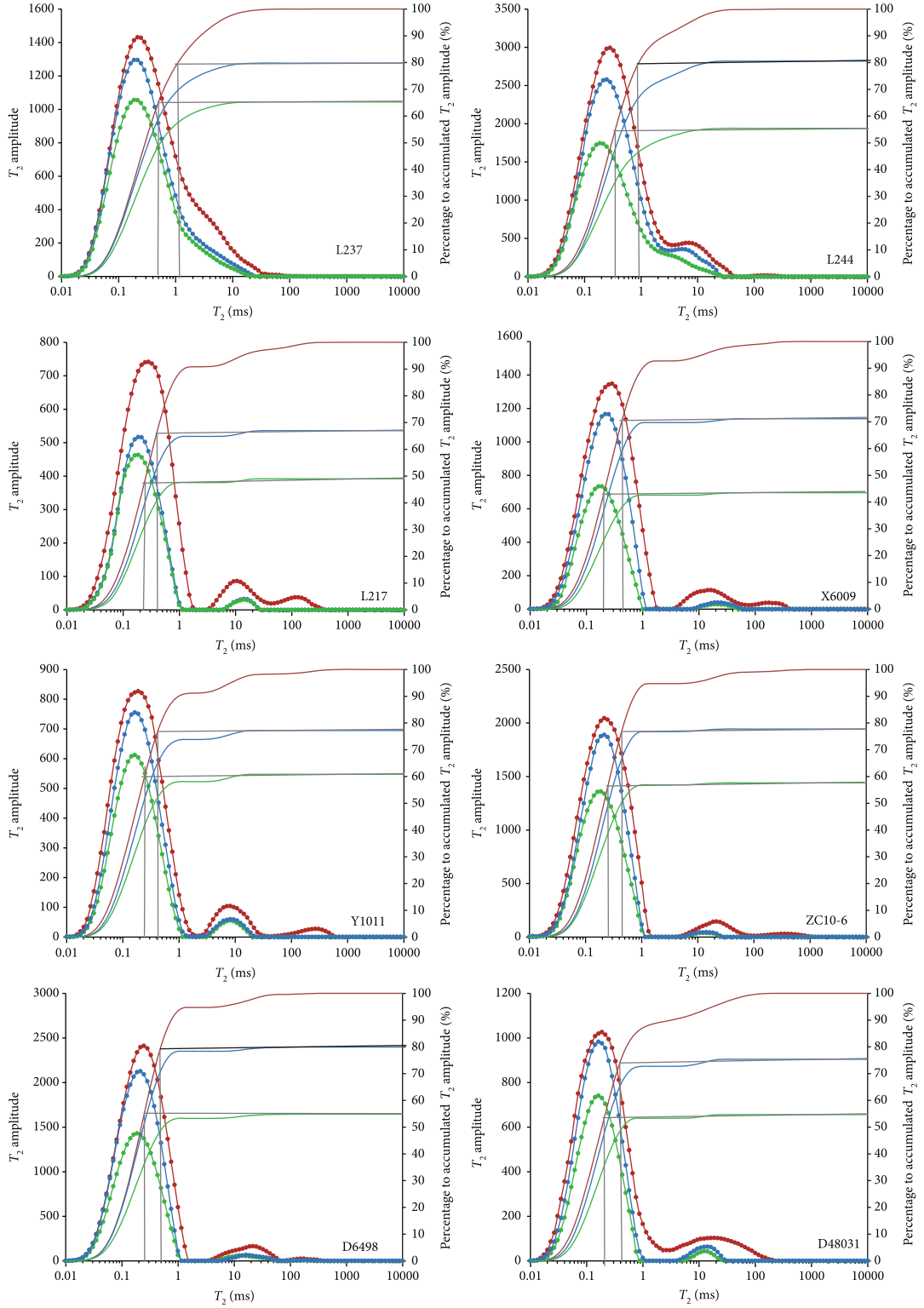

FIGURE 7: Distribution and accumulation curves of T_2 spectral amplitude under conditions at brine-saturated (red curves), centrifugating at 12000 rpm (blue curves), and heating to the threshold temperature (green curves).

medium-low maturity. The main mineral compositions of the shale are quartz, clay minerals, plagioclase, and potassium feldspar, followed by calcite, (iron) dolomite, pyrite, and minor amounts of mica and siderite. The high contents of siliceous minerals (quartz and feldspar), among brittle minerals, in the shales (38.4%–78.2%), facilitate natural fracture formation and subsequent fracturing. The sharp petrographic changes in the terrestrial shales and the fact that

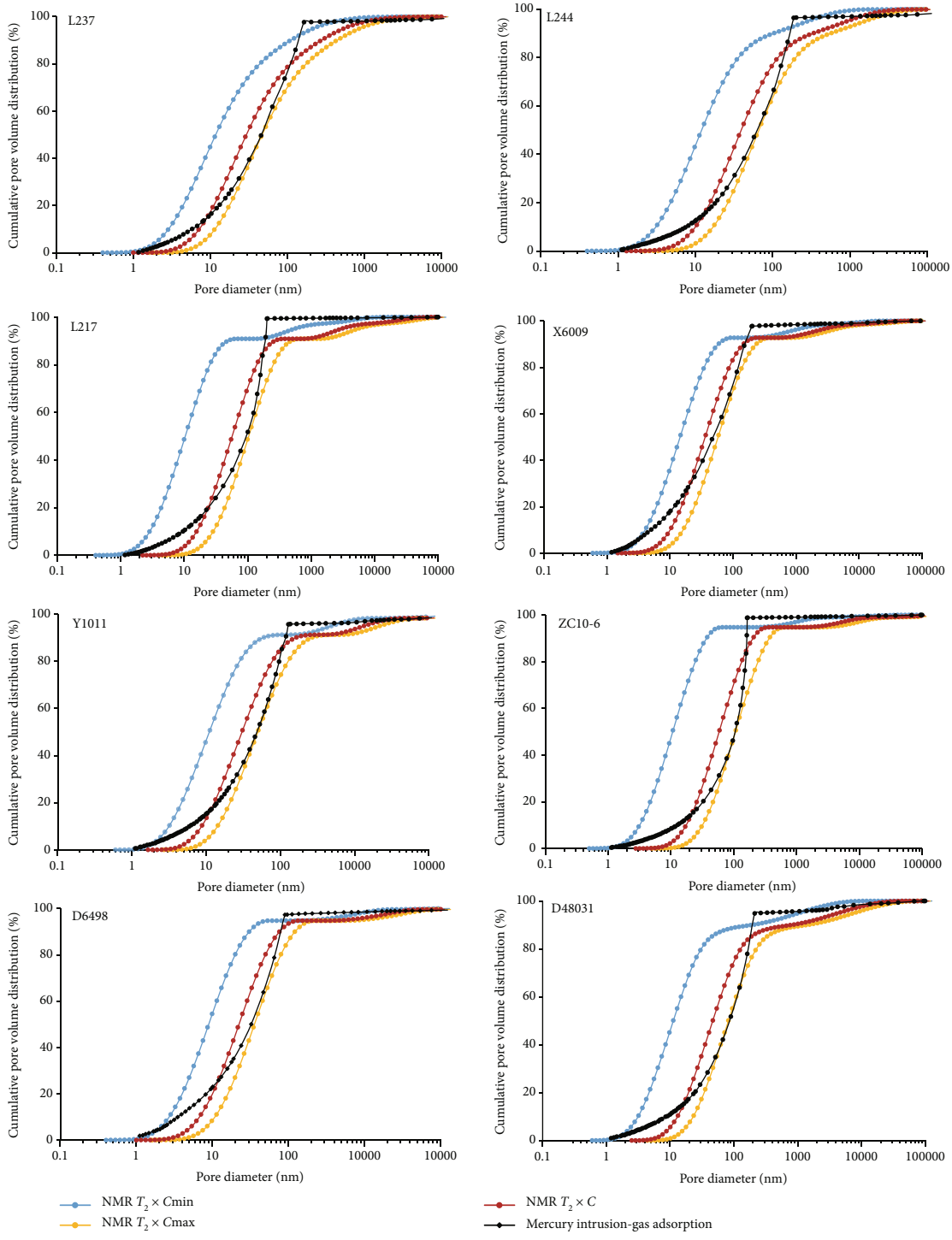

Figure 8: Determination of the C value based on the pore volume distribution curves by NMR and mercury intrusion combined with gas adsorption.

these eight shale samples were taken from different regions resulted in mineral compositions that varied significantly (Table 1).

The type, structure, and characteristics of pores and mineral composition of shale were observed and analyzed through thin section and (field emission) scanning electron microscopy. According to the existing classification of pore types in shale [10], the pores types in Zhangjiatan shale include mineral matrix, organic matter, and microfracture pores (Figure 2). Among them, the mineral matrix pores can be further divided into dissolution pores, pores between clay platelets, intercrystalline pores within pyrite framboids, and interparticle pores (Figure 2).

4.2. T_2 Spectra under Centrifugation. T_2 spectra of the brine-saturated samples and those after centrifugation are shown

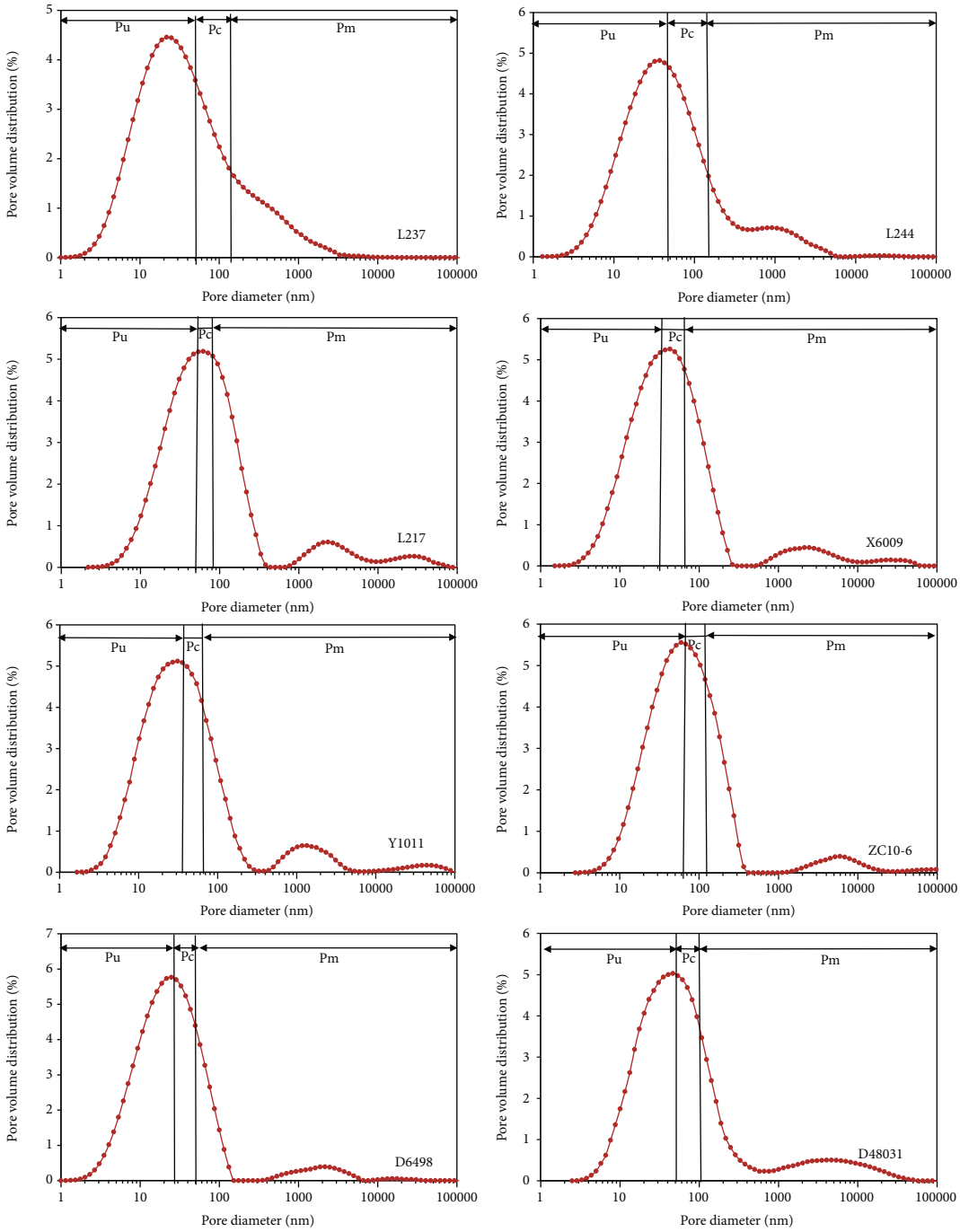

Figure 9: NMR pore size distribution curves showing pores with movable, capillary-bound, and unrecoverable fluids that denoted by P_m, P_c, and P_u, respectively.

in Figure 3. Comparing the T_2 spectra under saturation and those after centrifugation helps to analyze pore fluid transport during centrifugation. The T_2 spectrum distribution of the brine-saturated samples reflects the pore distributions of different pore sizes within the shales, and the integral areas represent the amounts of fluids within the total pore space of the shales. The T_2 signals of the eight shale samples under brine saturation generally show 2–3 peaks. More specifically, the peaks with large amplitudes are in the time range of 0.01–10 ms, whereas the peaks with smaller amplitudes are in the time range of 3–100 ms and 50–400 ms. Because fluids in small pores have faster relaxation than those in large pores, i.e., T_2 relaxation times are positively proportional to the corresponding pore sizes [30, 31], the T_2 spectra of the brine-saturated samples suggest that these shales have mostly tiny pores and few large pores.

As the centrifugal pressure increases, the signal amplitude of the T_2 spectrum after centrifugation decreases. In particular, the right peak decreases significantly, whereas the left peak decreases less, which indicates that the fluids

Table 3: C values converted from T_2 and minimum pore sizes for movable and capillary-bound fluids.

Samples	Depth (m)	T_{2-1} (ms)	T_{2-2} (ms)	C_{max}	C_{min}	C	P_m (nm)	P_c (nm)
L237	1176.9	1.10	0.50	160	40	100	110.0	50.0
L244	1314.0	1.01	0.36	220	40	130	131.3	46.8
L217	1379.7	0.40	0.25	400	40	220	88.0	55.0
X6009	1410.0	0.43	0.21	240	60	150	64.5	31.5
Y1011	1747.0	0.41	0.23	270	60	165	67.7	38.0
ZC10-6	2078.0	0.44	0.25	500	50	275	121.0	68.8
D6498	2230.5	0.49	0.25	160	40	100	49.0	25.0
D48031	2496.0	0.42	0.21	440	60	250	105.0	52.5

inside large pores are mostly movable. Furthermore, the T_2 spectra, as a whole, demonstrate a tendency to shift to the left, reflecting that the fluids gradually migrate from large pores to small pores. The difference between the cumulative signal amplitude curves of T_2 spectra under brine saturation and those after centrifugation is the movable fluid content in the pores of the shales. In the present study, the T_2 value (T_{2-1}) at the maximum centrifugal speed of 12000 rpm, which corresponds to a centrifugal pressure of 5.68 MPa, corresponds to cutoff values to differentiate movable fluids from bound fluids in the pores of the shales.

4.3. T_2 Spectra under Heating. However, even under a centrifugal pressure of 5.68 MPa (at 12000 rpm), the centrifugal force is not sufficient to remove all the fluids from the pores, and some fluids remain in the micropores. These remaining fluids are associated with the capillary-bound and unrecoverable fluids in the shales. Therefore, centrifugal separation only enables the calculation of the movable fluid saturation, but it does not allow the distinction between capillary-bound and unrecoverable fluids. Hence, after the centrifugation experiments, heat treatments were performed to distinguish between capillary-bound and unrecoverable fluids in the shales.

The T_2 spectra of the shales after heating are shown in Figure 4. Compared with those obtained at the centrifugal speed of 12000 rpm, the signal amplitudes of the heated shale samples decreased significantly. More specifically, the signal amplitudes of the T_2 spectra declined gradually as the temperature increased. The signal amplitude changes for the eight samples tested can be divided into two stages. In the first stage, five samples (L244, L237, Y1011, ZC10-6, and D6498) are heated to 40°C–90°C, and the signal amplitudes of the spectra declined rapidly. Additionally, in the second stage, i.e., at the temperature range from 90°C to 130°C, the signal amplitudes remained almost unchanged or exhibited little variation. As a result, 90°C was the critical temperature for the two stages. For the other three samples (L217, X6009, and D48031), the critical temperature was 115°C. This critical temperature dividing two phases of signal amplitude variations represents the minimum temperature at which the shale must be heated such that only unrecoverable fluids are retained. It is also the approximate minimum temperature at which all movable fluids in the pores will be evaporated [16]. This is because unrecoverable fluids are usually bound in tiny pores with relatively high capillary forces, and they are less able to flow compared to capillary-bound fluids. In the first phase of signal amplitude variations, the amplitude decreased rapidly as the temperature increased, suggesting that the residual capillary-bound fluids evaporate relatively quickly. However, in the second phase, only a small amount of clay-bound fluids could be evaporated at higher temperatures, and the vaporized water molecules confined in tiny pores could not escape but were instead condensed again into the liquid state because of attractive binding [32, 33].

Thus, the T_2 value at this critical temperature, defined as $T_{2-2,}$ can be used to distinguish between capillary bounds and unrecoverable fluids in the pores of the shales.

4.4. Pore Volume Distributions. According to the different pore size characterization ranges and accuracies of high-pressure mercury intrusion and N_2 adsorption experiments, the pore volume distributions and cumulative pore volume characteristics of the eight shale samples from the nanoscale to microscale were obtained as follows. Noteworthy is that the pore size classification system used by Zhang et al. and Lu et al. [34, 35], which divides pores into four types, i.e., micropores (<25 nm in diameter), small pores (25–100 nm in diameter), mesopores (100–1000 nm), and macropores (>1000 nm), was used to classify pore size in the shales. Those of macropores and mesopores are characterized by high-pressure mercury intrusion data, whereas small pores and micropores are analyzed using the experimental results by N_2 adsorption [36]. The results showed that the pore volume of the Zhangjiatan shale is mainly provided by micropores, small pores, and mesopores with pore sizes of 10–200 nm, and there were relatively fewer macropores. This finding is consistent with the pore volume distribution characteristics reflected by T_2 spectra under brine saturation described previously. Moreover, the cumulative pore volume of the eight shale samples obtained by combined mercury intrusion and gas adsorption exhibited a strong positive correlation with the porosity, especially permeability estimated by NMR (Table 2; Figure 5). This indicated that the full pore size distribution characterized by high-pressure mercury intrusion combined with N_2 adsorption is suitable as a basis for the conversion of T_2 relaxation times to pore sizes.

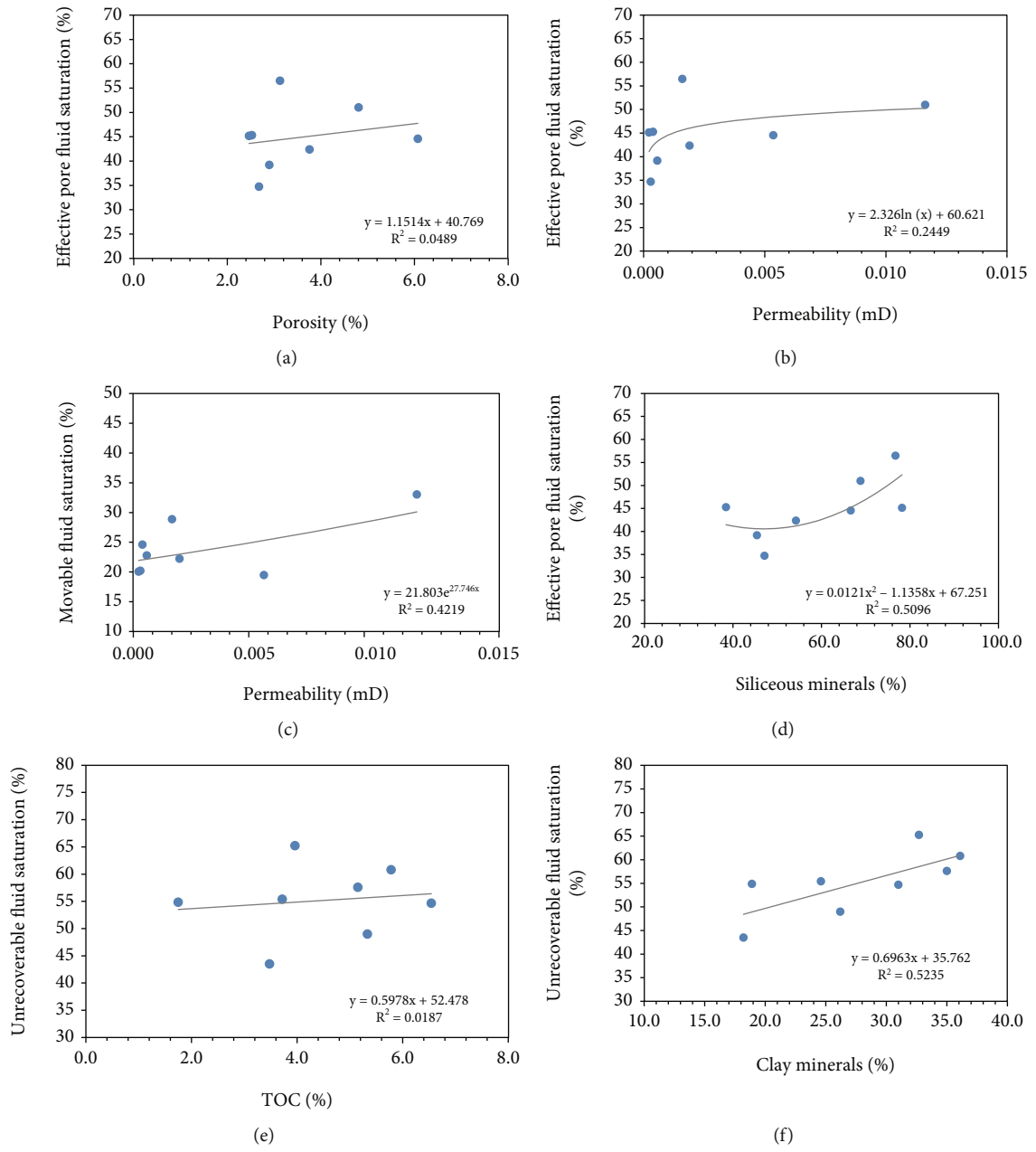

Figure 10: Correlation between pore fluid saturations and representative parameters for shale reservoir evaluation.

5. Discussion

5.1. Evaluation of Pore Fluid Movability. The distribution and accumulation curves of T_2 spectral amplitudes under brine saturation, centrifugation at 12000 rpm, and heating to the critical temperature are plotted from experimental NMR data. Because the NMR signal amplitudes of hydrogen atoms of the pore fluids are dimensionless and proportional to the pore fluid volumes [25], the accumulated T_2 spectral amplitude after normalization can be equated to the total pore fluid volume. Moreover, the projected intersections of the accumulation curve under brine saturation with that under centrifugation at 12000 rpm and that under critical heating can be projected vertically onto the axis of the T_2 relaxation time to derive the cutoff values T_{2-1} and T_{2-2} of the sample [25, 31, 37] (Figure 6). The T_2 cutoff values, namely, T_{2-1} and T_{2-2}, can be adopted to classify pore fluids as movable (when $T_2 > T_{2-1}$), capillary-bound (when $T_{2-1} > T_2 > T_{2-2}$), and unrecoverable fluids (when $T_{2-2} > T_2$).

Saturation levels of these three fluids are denoted by S_m, S_c, and S_u, respectively, and are calculated as shown in the following equations.

$$S_m = \frac{\int_{T_{2-1}}^{T_{max}} T_2 dT}{\int_{T_{min}}^{T_{max}} T_2 dT}, \quad (1)$$

$$S_c = \frac{\int_{T_{2-2}}^{T_{2-1}} T_2 dT}{\int_{T_{min}}^{T_{max}} T_2 dT}, \quad (2)$$

$$S_u = \frac{\int_{T_{min}}^{T_{2-2}} T_2 dT}{\int_{T_{min}}^{T_{max}} T_2 dT}, \quad (3)$$

where S_m is the movable fluid saturation, S_c is the capillary-bound fluid saturation, S_u is the unrecoverable fluid saturation, T_{2-1} is the T_2 cutoff value that distinguishes movable fluids from capillary-bound fluids, and T_{2-2} is the T_2 cutoff value that distinguishes capillary-bound fluids from unrecoverable fluids.

The final calculation results for T_{2-1} and T_{2-1} and S_m, S_c, and S_u are shown in Table 2. The ranges of T_{2-1} and T_{2-2} for the Zhangjiatan shale in the Ordos basin were 0.40–1.10 ms and 0.21–0.50 ms, respectively, whereas the corresponding average values were, respectively, 0.59 ms and 0.28 ms (Figure 7). The movable fluid saturation of the Zhangjiatan shale was 19.47–33.02% with an average of 23.91%, which is lower than those of sandstone and carbonate reservoirs [25, 38]. The capillary-bound fluid saturation equaled 14.53–27.62%, with an average of 20.94%. This revealed that small pores holding capillary-bound fluids accounted for a significant proportion of the total pore space.

As mentioned earlier, capillary-bound fluids are potentially movable fluids; thus, how this pore space can be effectively utilized during actual exploitation is critical to improving shale oil recovery. The unrecoverable fluid saturation of the Zhangjiatan shale was 43.51–65.26%, with an average of 55.15%. This reflects the poor fluid movability of the shale relative to that of conventional reservoirs.

Theoretical studies of NMR have shown that the T_2 spectral amplitude is proportional to the number of hydrogen nuclei, which is equal to the pore space volume within the sample. Therefore, NMR measurements can provide accurate porosity independent of mineralogical information [25]. In reservoir characterization, NMR porosity is typically calculated using an amplitude model based on the T_2 spectrum [25, 30, 39]. The porosity of pores holding different types of fluids can be calculated from the measured NMR total porosity (φ) of each shale sample and the corresponding saturation percentages of different pore fluids determined. The total porosity of the Zhangjiatan shale ranged from 2.47% to 6.08%, with an average of 3.55%. The movable fluid porosity φ_m, the capillary-bound fluid porosity φ_c, and the unrecoverable fluid porosity φ_u were within the ranges of 0.50–1.59%, 0.39–1.51%, and 1.35–3.37%, respectively (Table 2). Furthermore, NMR permeability estimation is based on a combination of experimental and theoretical models and their interrelationships. In particular, the Coates and SDR models are the most commonly used models for NMR permeability calculations [25]. However, the Coates model can more accurately estimate shale permeability and can be applied to both pore reservoirs and fractured reservoirs. Thus, in this research, the Coates model was chosen to calculate the permeability of the shale (Table 2).

5.2. Pore Size Distribution on the Basis of T_2 Spectra. Pore size is an important parameter reflecting the pore structures of shale. NMR did not only quantitatively characterize the full-size distributions of reservoir pores, but it also precisely revealed the pore fluid movability for pores of different sizes. Using the pore size distribution curves acquired by combining high-pressure mercury intrusions and gas adsorption experiments to calibrate the pore size distributions obtained by T_2 relaxation time spectra can more accurately and precisely portray the pore structures of shale reservoirs.

5.2.1. Conversion Model to Convert T_2 to Pore Size. In typical low-field NMR measurements, the T_2 spectra provide a wealth of information about the pore fluids in porous rocks. Typical T_2 relaxation times correlate with relaxation induced by the fluid itself, relaxation induced by the rock particle surface, and relaxation induced by molecular diffusion [25, 40]. However, when the pore is saturated with only unidirectional fluid and the magnetic field is homogeneous, free relaxation and diffusive relaxation are negligibly small relative to the surface relaxation. Therefore, a linear relationship between the pore fluid and T_2 can be established using NMR, as shown in the following equation.

$$\frac{1}{T_2} = \frac{1}{\rho_2}\frac{S}{V}, \quad (4)$$

where T_2 is the lateral relaxation time (ms), ρ_2 is the surface relaxation rate (nm/ms), and S/V is the specific surface area to volume of the pore (nm^{-1}).

From equation (4), it is clear that because small pores have larger S/V values, they have shorter T_2 relaxation times than large pores. Therefore, a relationship between the T_2 spectrum and the pore diameter d can be established.

$$\frac{S}{V} = \frac{F_s}{d}, \quad (5)$$

where F_S is the pore shape factor and d is the pore diameter (nm). Substituting equation (5) into equation (4) yields the following.

$$\frac{1}{T_2} = \rho_2 \frac{F_s}{d}. \quad (6)$$

By assuming that F_S and ρ_2 are constants for the same rock, equation (6) can be transformed into

$$d = C \times T_2. \quad (7)$$

According to equation (7), the T_2 relaxation time can be converted to the pore diameter d given a reasonable and optimal value of C.

5.2.2. Conversion of T_2 to Pore Size. The calibration method of Zhang et al. [41, 42] is used to obtain the C value based on the NMR, high-pressure mercury intrusion, and N_2 adsorption results of the eight shale samples, and the detailed procedure is summarized as follows.

Firstly, plot cumulative pore volume distribution (CPVD) curves based on T_2 spectra under brine saturation. Secondly, plot CPVD curves for full pore sizes based on high-pressure mercury intrusion combined with gas adsorption. Thirdly, determine the maximum C value: plot the CPVD curves for different C values based on the T_2 spectra. The maximum C value (C_{max}) is the value at which the curve is tangent to the rightmost end of the full pore size CPVD curve based on high-pressure mercury intrusion combined with gas adsorption. Then, determine the minimum C value: plot the CPVD curves for different C values based on the T_2 spectra. The minimum C value (C_{min}) is the C value at which the curve is tangent to the leftmost end of the full pore size CPVD curve given by high-pressure mercury intrusion combined with gas adsorption. Finally, determine the C value: the average of the C_{max} and C_{min} values is set as the final C value, and the NMR pore size distribution at the C value is calculated (Figure 8).

With the help of the NMR pore sizes calibrated by the above method, volume distribution curves for all different pore sizes were acquired for the eight samples of Zhangjiatan shale (Figure 9). The pores of the samples were then classified according to the pore size thresholds corresponding to the calculated T_2 cutoff values, namely, T_{2-1} and T_{2-2} ($P_{m\ min} = C * T_{2-1}$ and $P_{c\ min} = C * T_{2-2}$) as those with movable fluids P_m, those with capillary-bound fluids P_c, and those with unrecoverable fluids P_u.

In shale reservoirs, fluid flows occur mainly through systems of interconnected pore networks. From Figure 9, the pore size distribution controls the fluid transport through the pores. The movable fluids in the eight samples were mainly in macropores and mesopores, with a small amount in small pores. Furthermore, the proportion of movable fluids increased as the pore size increased, and almost all macropores hosted movable fluids. The minimum pore size values for pores to have movable fluid ($P_{m\ min}$) ranged from 49.0 nm to 131.3 nm. Furthermore, capillary-bound fluids were mainly in small pores and some mesopores. The minimum diameter of these pores ($P_{c\ min}$) was 25.0–68.8 nm, reflecting the relatively poor fluid movability. When the pore size was below this threshold, mainly unrecoverable fluids were stored in the pores of interest. Unrecoverable fluids were mainly stored in micropores and small pores, and mesopores and macropores contained almost no unrecoverable fluids (Table 3).

5.3. Controlling Factors of Pore Fluid Movability in Zhangjiatan Shale. There are many factors influencing the pore fluid movability of rocks. Generally, given the better physical properties of the reservoirs and more developed pore structures, the movable fluid saturation was higher. The relationships of effective pore fluid saturation ($S_m + S_c$) with porosity (φ) and permeability K for Zhangjiatan shale are plotted according to Table 2 (Figures 10(a) and 10(b)). From the curves, the correlation between effective pore fluid saturation and porosity was nonsignificant. On the contrary, there was a relatively good positive correlation between effective pore fluid saturation and permeability. In particular, the movable fluid saturation had a stronger correlation with permeability (Figure 10(c)). This is primarily because porosity can only characterize the size of the reservoir space, but it does not reflect the pore connectivity. In addition, the pore structures of shales are more complex than those of conventional reservoirs. The above analysis shows that the dominant contributors to the porosity of the eight shale samples are micropores and small pores, which mainly control unrecoverable fluids, such that the overall effect of porosity on fluid movability is small. In contrast, permeability is a parameter that characterizes the ability of the rock itself to allow fluid passage, for shales with higher effective pore fluid saturation, especially movable fluid saturation. This indicates better pore connectivity and percolation capacity, thereby resulting in greater permeability.

The mineral compositions of the Zhangjiatan shale in the Ordos basin are dominated by quartz, feldspar, and clay minerals (Table 2). Among them, the contents of siliceous minerals (quartz and feldspar) exhibited strong correlations with the effective pore fluid saturation (Figure 10(d)). This is first because high quartz and feldspar contents in clastic grains with high-pressure resistance make interparticle pores more likely to be preserved, and interparticle pores in shales contribute more to the effective pore network than intragrain pores [10]. At the same time, hydrocarbon production and transportation in shales produce acidic fluids, such as organic acids and CO_2. This leads to the dissolution of feldspars and further increases pore space and connectivity. The second reason is that quartz and feldspar minerals are more brittle and microfracture easily, and increased pore connectivity easily occurs in these minerals.

The correlations of unrecoverable fluid saturation with TOC and that between clay mineral content for the Zhangjiatan shale were established separately (Figures 10(e) and 10(f)). The unrecoverable pore fluid saturation of the medium-low-maturity Zhangjiatan shale had a weak correlation with TOC but a strong positive correlation with clay minerals. In addition, the above analysis revealed that the unrecoverable fluids were mainly in tiny pores. This indicates that the tiny pores in the medium-low-maturity shale in the section mostly exist because of clay minerals. Furthermore, the organic matter pore development in the shale is poor. These are in high contrast to high-maturity shales where organic matter pore development and micropores mainly exist because of the organic matter present [43].

6. Conclusion

In order to quantify pore size and movable fluid distribution of the Zhangjiatan shale of Upper Triassic Yanchang Formation in the Ordos basin, core plugs from eight boreholes were measured in a series of NMR, MIP, and N_2 gas adsorption experiments to determine the pore structure and pore fluid transport during the processes of centrifuging and heating. The main findings are summarized as follows:

(1) The movable, capillary-bound, and unrecoverable fluid saturation values of the Zhangjiatan shale were 19.47–33.02%, 14.53–27.62%, and 43.51–65.26%, respectively. The movable fluid saturation was lower

than those of tight sandstone and carbonate reservoirs. Moreover, capillary-bound fluids are potentially movable fluids, and how to use the pore space holding these fluids in practice is important to improve the recovery of shale oil

(2) The movable fluids in the pores of the Zhangjiatan shale were mainly found in macropores and mesopores, with a small amount in small pores, and the minimum diameter of these pores was 49.0–131.3 nm. Furthermore, capillary-bound fluids were mainly located in small pores and some mesopores, and the minimum diameter of these pores was 25.0–68.8 nm. Lastly, unrecoverable fluids were mainly in micropores and small pores, whereas mesopores and macropores contained almost no unrecoverable fluids

(3) Unlike the high-maturity shales where tiny pores are mainly formed thanks to organic matter, the medium-low-maturity Zhangjiatan shale has a weak unrecoverable fluid saturation-TOC correlation of unrecoverable fluid saturation and a strong positive unrecoverable fluid saturation-clay mineral correlation. These results suggest that unrecoverable fluid saturation of the tiny pores in medium-low-maturity shales is mostly from clay minerals, whereas organic matter pores are poorly developed

Data Availability

The data used to support the findings of this study are included within the article.

Disclosure

We thank the Shanxi Yanchang Petroleum (Group) Corp., Ltd. for permission to publish this work.

Conflicts of Interest

The authors declare that they have no conflicts of interest.

Acknowledgments

This work was made possible by grants from the Chinese National Major Fundamental Research Developing Project (2017ZX05008-004-004); the Science and Technology Planning Project of Shanxi Yanchang Petroleum (Group) Corp., Ltd.; the Key Scientific and Technological Innovation Team Project in Shaanxi Province; and the MOST Special Fund from the State Key Laboratory of Continental Dynamics and Department of Geology at Northwest University.

References

[1] J. A. Breyer, "Shale reservoirs—giant resources for the 21st century," *AAPG Memoir*, vol. 97, article 519, 2012.

[2] R. F. Aguilera and M. Radetzki, "Shale gas and oil: fundamentally changing global energy markets," *Oil and Gas Journal*, vol. 111, pp. 54–61, 2013.

[3] R. F. Aguilera and M. Radetzki, "The shale revolution: global gas and oil markets under transformation," *Mineral Economics*, vol. 26, no. 3, pp. 75–84, 2014.

[4] A. Furmann, M. Mastalerz, D. Bish, A. Schimmelmann, and P. K. Pedersen, "Porosity and pore size distribution in mudrocks from the Belle Fourche and Second White Specks Formations in Alberta, Canada," *AAPG Bulletin*, vol. 100, no. 8, pp. 1265–1288, 2016.

[5] L. U. Shuangfang, X. U. E. Haitao, W. A. N. G. Min et al., "Several key issues and research trends in evaluation of shale oil," *Acta Petrolei Sinica*, vol. 37, no. 10, pp. 1309–1322, 2016.

[6] C. M. Agyingi, N. C. Tangko, and E. Eseme, "Bulk petroleum geochemistry of shales from the onshore Rio del Rey Basin, Cameroon," *Energy Geoscience*, vol. 3, no. 2, pp. 111–119, 2022.

[7] R. Rezaee, *Fundamentals of Gas Shale Reservoirs*, John Wiley & Sons, New York, 2015.

[8] G. Fenglin, S. Yan, L. Zhikai et al., "Development characteristics of organic pore in the continental shale and its genetic mechanism: a case study of Shahezi Formation shale in the Changling fault depression of Songliao Basin," *Acta Petrolei Sinica*, vol. 40, no. 9, pp. 1030–1044, 2019.

[9] S. Zhou, H. Liu, G. Yan, H. Xue, and W. Guo, "NMR research of movable fluid and T_2 cutoff of marine shale in South China," *Oil &Gas Geology*, vol. 37, no. 4, pp. 612–616, 2016.

[10] R. G. Loucks, R. M. Reed, S. C. Ruppel, and U. Hammes, "Spectrum of pore types and networks in mudrocks and a descriptive classification for matrix-related mudrock pores," *AAPG Bulletin*, vol. 96, no. 6, pp. 1071–1098, 2012.

[11] L. Christian, K. E. Gubbins, and N. Quirke, "Pore size distribution analysis of microporous carbons: a density functional theory approach," *The Journal of Physical Chemistry*, vol. 97, no. 18, pp. 4786–4796, 1993.

[12] C. H. Sondergeld, R. J. Ambrose, C. S. Rai, and J. Moncrieff, "*Micro-structural studies of gas shales*," in *SPE Unconventional Gas Conference*, Pittsburgh, Pennsylvania, USA, February 2010.

[13] M. Mehamed and I. El-monier, "Shale characteristics impact on nuclear magnetic resonance (NMR) fluid typing methods and correlations," *Petroleum*, vol. 2, no. 2, pp. 138–147, 2016.

[14] Q. R. Passey, K. M. Bohacs, W. L. Esch, R. Klimentidis, and S. Sinha, "From oil-prone source rock to gas-producing shale reservoir-geologic and petrophysical characterization of unconventional shale gas reservoirs," in *International Oil and Gas Conference and Exhibition in China*, Beijing, China, June 2010.

[15] P. Zhang, *Research on shale oil reservoir, occurrence and movability using nuclear magnetic resonance (NMR)*, China University of Petroleum, East China, 2019.

[16] M. N. Testamanti and R. Rezaee, "Determination of NMR T_2 cut-off for clay bound water in shales: a case study of Carynginia Formation, Perth Basin, Western Australia," *Journal of Petroleum Science and Engineering*, vol. 149, pp. 497–503, 2017.

[17] Z. H. A. O. Wenzhi, H. U. Suyun, H. O. U. Lianhua et al., "Types and resource potential of continental shale oil in China and its boundary with tight oil," *Petroleum Exploration and Development*, vol. 47, pp. 1–11, 2020.

[18] J. Wang and J. Wang, "Low-amplitude structures and oil-gas enrichment on the Yishaan Slope, Ordos Basin," *Petroleum Exploration and Development*, vol. 40, no. 1, pp. 52–60, 2013.

[19] H. Yang and W. Z. Zhang, "Leading effect of the seventh member high-quality source rock of Yanchang Formation in Ordos Basin during the enrichment of low-penetrating oil-gas accumulation (in Chinese)," *Geochimica*, vol. 34, no. 2, pp. 147–154, 2005.

[20] J. H. Fu, X. Y. Liu, S. X. Li, Q. H. Guo, X. P. Zhou, and W. W. Yang, "Discovery and resource potential of shale oil of Chang 7 member, Triassic Yanchang Formation, Ordos Basin (in Chinese)," *China Petroleum Exploration*, vol. 26, no. 5, pp. 1–11, 2021.

[21] Q. F. Kong, "The organic maceral characteristic of Yanchang source rock in Ordos Basin (in Chinese)," *Xinjiang Petroleum Geology*, vol. 28, no. 2, pp. 163–166, 2007.

[22] S. P. Ma, Y. L. Qi, X. B. Zhang et al., "Geochemical characteristics and hydrocarbon generation potential of the source rocks in Yanchang Formation, Xifeng Oilfield, Ordos Basin, NW China (in Chinese)," *Petroleum Exploration and Development*, vol. 32, no. 32, pp. 51–54, 2005.

[23] W. H. Zhang, H. Yang, J. F. Zhang, and J. Ma, "Leading effect of high class source rock of Chang 7 in Ordos Basin on enrichment of low permeability oil–gas accumulation Hydrocarbon generation and expulsion mechanism (in Chinese)," *Petroleum Exploration and Development*, vol. 33, no. 3, pp. 289–293, 2006.

[24] M. Y. Nikolaev and A. V. Kazak, "Liquid saturation evaluation in organic-rich unconventional reservoirs: a comprehensive review," *Earth-Science Reviews*, vol. 194, pp. 327–349, 2019.

[25] G. R. Coates, L. Z. Xiao, and M. G. Prammer, *NMR Logging Principles and Applications*, Houston, Gulf Publishing Company, Halliburton Energy Services, 1999.

[26] A. A. Hinai, R. Rezaee, L. Esteban, and M. Labani, "Comparisons of pore size distribution: a case from the Western Australian gas shale formations," *Journal of Unconventional Oil and Gas Resources.*, vol. 8, pp. 1–13, 2014.

[27] R. Rezaee, A. Saeedi, and B. Clennell, "Tight gas sands permeability estimation from mercury injection capillary pressure and nuclear magnetic resonance data," *Journal of Petroleum Science and Engineering*, vol. 88-89, pp. 92–99, 2012.

[28] E. W. Washburn, "The dynamics of capillary flow," *Physical Review*, vol. 17, no. 3, article 273, 1921.

[29] X. Tang, Z. Jiang, Z. Li et al., "The effect of the variation in material composition on the heterogeneous pore structure of high-maturity shale of the Silurian Longmaxi formation in the southeastern Sichuan Basin, China," *Journal of Natural Gas Science and Engineering*, vol. 23, pp. 464–473, 2015.

[30] K. J. Dunn, D. J. Bergman, and G. A. Latorraca, *Nuclear Magnetic Resonance Petrophysical and Logging Applications*, Pergamon, Elsevier Science, Oxford, 2002.

[31] H. Westphal, I. Surholt, C. Kiesl, H. F. Thern, and T. Kruspe, "NMR measurements in carbonate rocks: problems and an approach to a solution," *Pure and Applied Geophysics*, vol. 162, no. 3, pp. 549–570, 2005.

[32] K. S. W. Gregg and S. J. Sing, *Adsorption, surface area, and porosity*, Academic Press, London& New York, 1982.

[33] F. Rouquerol, J. Rouquerol, and K. Sing, *Adsorption by Powders and Porous Solids: principles, Methodology and Applications*, Academic Press, London, 1999.

[34] P. Zhang, S. Lu, J. Li, H. Xue, W. Li, and P. Zhang, "Characterization of shale pore system: a case study of Paleogene Xin'gouzui Formation in the Jianghan basin, China," *Marine and Petroleum Geology*, vol. 79, pp. 321–334, 2017.

[35] L. U. Shuangfang, L. I. Junqian, P. Zhang et al., "Classification of microscopic pore-throats and the grading evaluation on shale oil reservoirs," *Petroleum Exploration and Development*, vol. 45, no. 3, pp. 452–460, 2018.

[36] U. Kuila and M. Prasad, "Specific surface area and pore-size distribution in clays and shales," *Geophysical Prospecting*, vol. 61, no. 2, pp. 341–362, 2013.

[37] Y. Yao, D. Liu, Y. Che, Z. D. Tang, S. Tang, and W. Huang, "Petrophysical characterization of coals by low-field nuclear magnetic resonance (NMR)," *Fuel*, vol. 89, no. 7, pp. 1371–1380, 2010.

[38] D. Ren, H. Zhang, Z. Wang, B. Ge, D. Liu, and R. Zhang, "Experimental study on microscale simulation of oil accumulation in sandstone reservoir," *Frontiers in Physics*, vol. 176, no. 10, article 841989, 2022.

[39] H. Xu, D. Tang, J. Zhao, and S. Li, "A precise measurement method for shale porosity with low-field nuclear magnetic resonance: a case study of the Carboniferous-Permian strata in the Linxing area, eastern Ordos Basin, China," *Fuel*, vol. 143, pp. 47–54, 2015.

[40] R. L. Kleinberg and M. A. Horsfield, "Transverse relaxation processes in porous sedimentary rock," *Journal of Magnetic Resonance*, vol. 88, no. 1, pp. 9–19, 1990.

[41] Y. G. Zhang, *Study on micro geological feature of tight sandstone gas reservoir at eastern part of Sulige gas field, Ordos basin, [M.S. thesis]*, Northwest University, Washington, 2014.

[42] P. Zhang, S. Lu, J. Li, C. Chen, J. Zhang, and H. Xue, "Petrophysical characterization of oil-bearing shales by low-field nuclear magnetic resonance (NMR)," *Marine and Petroleum Geology*, vol. 89, pp. 775–785, 2018.

[43] Y. Song, F. Gao, X. Tang, L. Chen, and X. Wang, "Influencing factors of pore structure differences between marine and terrestrial shale reservoirs," *Acta Petrolei Sinica*, vol. 41, no. 12, pp. 1501–1512, 2020.